DOI: 10.1002/chem.200601092

One-Step Fabrication and High Photocatalytic Activity of Porous TiO_2 Hollow Aggregates by Using a Low-Temperature Hydrothermal Method Without Templates

Zhaoyang Liu,*[a] Darren D. Sun,*[a] Peng Guo,[b] and James O. Leckie[c]

Abstract: Porous TiO_2 hollow aggregates have been synthesized on a large scale by means of a simple hydrothermal method without using any templates. The as-prepared products were characterized by means of field emission scanning electron microscopy, XRD, TEM, nitrogen adsorption, UV/Vis diffuse reflectance spectroscopy, and FTIR spectroscopy. The photocatalytic activity of the aggregates was demonstrated through the photocatalytic degradation of Rhodamine B. Structural characterization indicates that the porous TiO_2 aggregates are 500–800 nm in diameter and display mesoporous structure. The average pore sizes and BET surface areas of the aggregates are 12 nm and 168 $m^2 g^{-1}$, respectively. Optical adsorption investigations show that the aggregates possess an optical band-gap energy of 3.36 eV. The as-prepared products were substantially more effective photocatalysts than the commercially available photocatalyst P25. The dye degradation rate of the porous TiO_2 hollow aggregates is more than twice that of P25. The high photoactivities of the aggregates can be attributed to the combined effects of several factors, namely, large surface areas, the existence of mesopores, and the high band-gap energy. In addition, the as-prepared products can be easily recycled.

Keywords: aggregation · microporous materials · nanostructures · photocatalysis · titanium dioxide

Introduction

Nanosized TiO_2 is the most popular photocatalyst for the elimination of pollutants.[1] However, application of these nanosized TiO_2 materials is challenging, in particular, when removing contaminants from water. For commercial applications as a photocatalyst, a material must have superior photocatalytic activity, and be easily synthesized and recovered. TiO_2 nanoparticles might re-pollute the water owing to the tremendous difficulties in separation and recovery. In addition, TiO_2 nanoparticles often show lower efficiencies owing to aggregation problems.[2] Immobilizing TiO_2 nanofilms on supporting materials has been frequently adopted to improve reclamation procedures.[3] Unfortunately, a significant loss in the surface area by using this technique limits the photocatalytic efficiency.

Nanostructured TiO_2 exhibits superior photocatalytic efficiency relative to conventional bulk materials as a result of its large surface area and is one of the most intensively researched substances in recent years.[4,5] To enhance the photocatalytic ability, various morphologies of nanostructured TiO_2, including porous particles, fibers, tubes, and spheres, have been prepared by means of chemical or physical methods.[6–11] Micro- and nanostructures with hollow interiors have attracted significant interest owing to their many attractive characteristics, such as low density, economical use of materials, and high surface-to-volume ratios. Recently, Li and co-workers described a sol–spraying–calcination method to fabricate a new type of TiO_2 microsphere photocatalyst with a particle size of 30–160 μm.[12] Xie and co-workers reported the fabrication of crystallized rutile phase TiO_2 hollow spheres by using potassium titanium oxalate as the precursor and by employing a simple hydrothermal method, although the photocatalytic performance was lower owing to the rutile phase.[13] More recently, Chen and co-workers fabricated long TiO_2 hollow fibers with mesoporous walls,

[a] Dr. Z. Liu, Prof. Dr. D. D. Sun
School of Civil and Environmental Engineering
Nanyang Technological University, Block N1, Nanyang Avenue
Singapore 639798 (Singapore)
Fax: (+65) 679-10-676
E-mail: Liu_zhaoyang2003@yahoo.com
DDSun@ntu.edu.sg

[b] Dr. P. Guo
Institute of Chemistry, Chinese Academy of Sciences
Zhongguancun, Beijing, 100080 (China)

[c] Prof. Dr. J. O. Leckie
Department of Civil and Environmental Engineering
Stanford University, Stanford, California 94305-4020 (USA)

which showed higher photocatalytic activity, by means of a sol–gel process combined with a two-capillary spinneret electrospinning technique and by using a triblock copolymer as a pore template.[14] However, most of the existing methods use intrinsically costly precursors, templates, and high-temperature procedures, or show lower photocatalytic performance. Therefore, the development of cost-effective methods suitable for the large-scale synthesis of TiO_2 nanostructured materials with a high photocatalytic activity and easy recycling is essential for their practical application.

In this paper, a simple one-step, low-temperature hydrothermal method without employing any organic or inorganic templates was used to produce nanostructured TiO_2 hollow aggregates with porous walls. The advantages of the present products are as follows:

1) High surface-to-volume ratios with effective prevention of further aggregation of the nanoparticle clusters.
2) Higher redox potentials with an increase in band-gap energy as a result of the so-called 'quantum size effect'.
3) The excellent photocatalytic degradation efficiency of Rhodamine B (RhB) compared with commercial P25 TiO_2 nanoparticles.
4) Easy to recover and recycle owing to the larger diameters of the nanostructured porous TiO_2 hollow aggregates.

Results and Discussion

Field emission scanning electron microscopy (FESEM) analyses were performed to examine the morphology of the as-prepared samples. Figures 1a–c show the FESEM images of the porous TiO_2 hollow aggregates at different magnifications. Figure 1a shows a low-magnification FESEM image of the sample, which indicates that the aggregates are composed of a large quantity of nanoparticles. The diameter of these nanoparticle aggregates is about 500–800 nm. A typical FESEM image of a single aggregate is presented in Figure 1b, in which the hollow interior of the aggregate is clearly visible. The porous structure of the TiO_2 nanoparticle aggregates can be seen more easily from FESEM images recorded at a higher magnification (Figure 1c). As shown in Figure 1c, the sample exhibits a unique porous surface. The hollow structure of the TiO_2 nanoparticle aggregates was further confirmed by means of TEM as shown in Figure 1d.

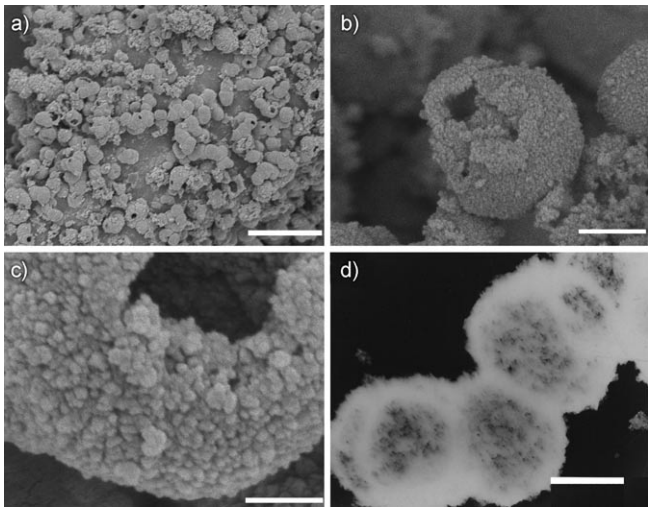

Figure 1. a–c) FESEM and d) TEM images of the porous TiO_2 hollow aggregates prepared by one-step hydrothermal treatment at 160 °C for 6 h, recorded at different magnifications. The scale bars for a)–d) are 5 μm, 500 nm, 100 nm, and 500 nm, respectively.

The XRD patterns for the porous TiO_2 hollow aggregates obtained hydrothermally from 120 to 180 °C are shown in Figure 2. The intensities of the diffraction peaks increased with increasing hydrothermal temperatures. The strong sharp diffraction peaks of the two samples at 160 and 180 °C are very similar and are in good agreement with an anatase phase (JCPDS file no. 21-1272). This result illustrates that heating to 160 °C is sufficient to produce a full anatase phase by using this method. The average crystal size of the sample (D in nanometers) has been estimated by using Scherrer's formula, which is shown in Equation (1):

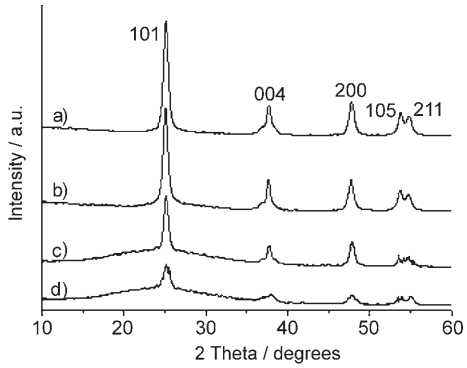

Figure 2. XRD patterns of the as-prepared porous TiO_2 hollow aggregates obtained by means of a one-step hydrothermal method for 6 h at different temperatures: a) 180, b) 160, c) 140, and d) 120 °C.

$$D = \frac{0.89\lambda}{B(2\theta)\cos\theta} \quad (1)$$

in which $B(2\theta)$ is the width of the XRD peak at half-peak height in radians, λ is the X-ray wavelength in nanometers, and θ is the angle between the incident and diffracted beams in degrees. The crystal size of the porous TiO_2 hollow aggregates was estimated to be around 13 nm.

The optical band gaps of the porous TiO_2 hollow aggregates were studied by means of UV/Vis optical absorbance spectra (Figure 3). The band-gap energies can be estimated from a plot of $\sqrt{h\nu\alpha}$ versus photon energy ($h\nu$).[15] The intercept of the tangent to the plot will give a good approximation of the indirect band-gap energies of the samples. The

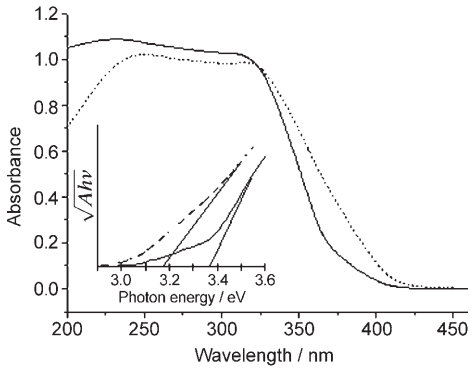

Figure 3. UV/Vis absorbance spectra of the porous TiO_2 hollow aggregates prepared hydrothermally at 160 °C (——) and of P25 TiO_2 (•••••). The inset shows the plot of $\sqrt{Ahv}$ versus photon energy (hv).

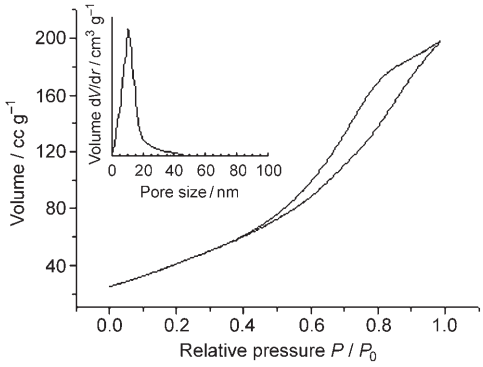

Figure 4. Nitrogen adsorption–desorption isotherm of the porous TiO_2 hollow aggregates prepared hydrothermally at 160 °C. The inset shows its BJH pore size distribution curve.

relationship between the absorption coefficient (α) and incident photon energy (hv) can be written as shown in Equation (2):

$$\alpha = \frac{B_i(hv - E_g)}{hv} \qquad (2)$$

in which B_i is the absorption constant for indirect transitions. As absorbance (A) is proportional to the absorption coefficient (α), we substituted α by A. Plots of $\sqrt{Ahv}$ versus (hv) are presented in the inset of Figure 3. The band-gap energy for the porous TiO_2 hollow aggregates was estimated to be $E = 3.36$ eV, which is higher than that of P25 TiO_2 ($E = 3.18$ eV), which has a crystal size of about 25 nm. The obvious blueshift of the optical band gap might be a result of the smaller average crystal size of the porous TiO_2 hollow aggregates; this is the quantum-size effect.

The surface area and porosity of the porous TiO_2 hollow aggregates were investigated by using nitrogen adsorption and desorption isotherms (shown in Figure 4). The isotherms are typical type IV-like with a type H2 hysteretic loop, which indicates the presence of mesoporous materials according to IUPAC classification.[16] The plot of the pore size distribution (inset in Figure 4) was determined by using the Barrett–Joyner–Halenda (BJH) method from the desorption branch of the isotherm; this shows that these TiO_2 aggregates clearly have mesoporous structure. The average pore diameter of the TiO_2 aggregates is 12 nm and the BET surface areas are about 168 $m^2 g^{-1}$.

The FTIR spectrum of the porous TiO_2 hollow aggregates is shown in Figure 5. The absorbances between $\tilde{\nu} = 500$ and 900 cm^{-1} originate from TiO_2.[17] The OH bending and stretching modes can be seen at 1640 and 3400 cm^{-1}, respectively;[18] this surface hydroxylation is very advantageous for the photocatalytic activity of the anatase-phase crystals because it provides higher capacity for oxygen adsorption.[19] There are no other bands in the spectrum, which indicates that no precursor residues reside in the porous TiO_2 hollow aggregates after washing the sample with distilled water.

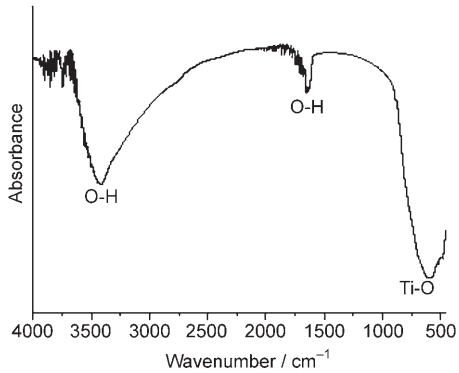

Figure 5. FTIR spectrum of the porous TiO_2 hollow aggregates prepared hydrothermally at 160 °C.

To explore the formation mechanism of hollow interiors, an experiment was performed by adopting a similar process for the preparation of porous TiO_2 hollow aggregates but without using NH_4F. Only solid TiO_2 aggregates were obtained without NH_4F, as shown in Figure 6, which indicates that the formation of porous TiO_2 hollow aggregates can be attributed to the HF generated during the hydrothermal process. HF is a corrosive chemical etchant, which was formed in situ as a hydrolysis product of NH_4F during the production of TiO_2. This process will create a localized HF rich zone in the area around the TiO_2 particle. It is well-known that the hydrothermal process is a dissolution–re-

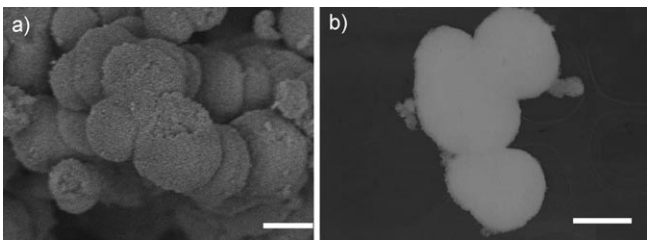

Figure 6. a) FESEM and b) TEM images of the as-prepared TiO_2 solid aggregates prepared hydrothermally without NH_4F under the same conditions as those of the porous TiO_2 hollow aggregates. The scale bars are both 500 nm.

deposition process. The large hollow interiors are gradually produced by repeating two steps, chemical etching of the TiO_2 solid particle by HF followed by recrystallization of its surface. In another experiment in which NH_4F was replaced by NH_4Cl to avoid HF formation during the synthesis, no hollow structures could be found in the final products. This experiment further confirms the crucial role of NH_4F for the formation of hollow structures.

To demonstrate the potential applicability of the present porous TiO_2 hollow aggregates for the removal of contaminants from wastewater, we investigated their photocatalytic activity relative to that of a commercial photocatalyst (Degussa P25 TiO_2) by employing the photocatalytic degradation of RhB as a test reaction. The characteristic absorption of RhB at $\lambda = 553$ nm was chosen to monitor the photocatalytic degradation process. Figure 7 shows the absorption

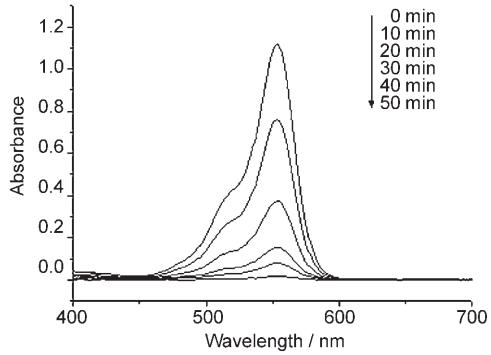

Figure 7. Absorption spectra of a solution of RhB (1.0×10^{-5} M, 100 mL) at room temperature in the presence of 30 mg of the porous TiO_2 hollow aggregates and under exposure to UV light ($\lambda = 254$ nm).

spectrum of an aqueous solution of RhB exposed to UV light for various time periods. The absorption peak at $\lambda = 553$ nm diminishes gradually as the UV exposure time increases, and completely disappears after about 50 min. No new absorption bands appear in either the visible or ultraviolet regions, which indicates the complete photocatalytic degradation of RhB during that reaction.

The changes in RhB concentration and total organic content (TOC) over the course of the photocatalytic degradation reaction are shown in Figure 8, which clearly indicates that with identical UV-light exposure, the porous TiO_2 hollow aggregates show much greater activity than that of commercial P25. The photocatalytic degradation of RhB in the process follows first-order kinetics. The apparent rate constant ($k = 0.086\ min^{-1}$) for the TiO_2 aggregates was more than twice that of commercial P25 ($k = 0.041\ min^{-1}$). The TOC curves in Figure 8 also show that the photocatalytic decomposition rate of the TiO_2 aggregates was superior to that of commercial P25. The higher photocatalytic activity of the porous TiO_2 hollow aggregates can be explained by considering several factors:

1) The larger specific surface area (porous TiO_2 hollow aggregates ca. $168\ m^2g^{-1}$ versus Degussa P25 powder ca. $45\ m^2g^{-1}$); hence, there are more reactant adsorption/desorption sites for catalytic reaction.
2) The prevention of the unwanted aggregation of the nanoparticles clusters, which is also helpful in maintaining the high active surface area.
3) The highly porous structure, which allows rapid diffusion of various reactants and products during the reaction.
4) The smaller crystal size, which means more powerful redox ability owing to the quantum-size effect; moreover, the smaller crystal sizes are also beneficial for the separation of the photogenerated hole and electron pairs.

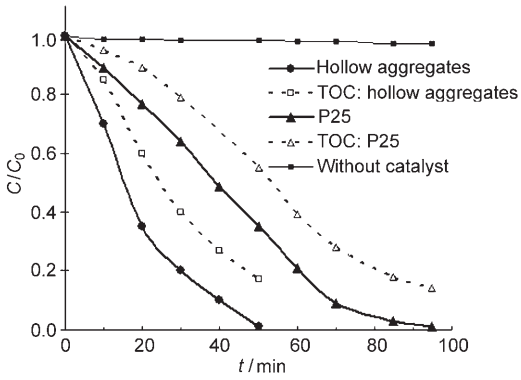

Figure 8. Changes in RhB concentration (C) and TOC over the course of the photocatalytic degradation of RhB (1.0×10^{-5} M) in the presence of various photocatalysts ($0.3\ gL^{-1}$) and under exposure to UV light ($\lambda = 254$ nm).

The porous TiO_2 hollow aggregates are a kind of heterogeneous photocatalyst that can be easily recycled by means of a simple filtration step. After seven cycles of the photocatalytic degradation of RhB, the catalyst did not exhibit any significant loss of photocatalytic activity, as shown in Figure 9, which indicates the excellent stability that is important for its practical application.

Conclusion

In conclusion, porous TiO_2 hollow aggregates were successfully fabricated by employing a facile one-step low-temperature hydrothermal process without using any templates. This method is very simple and easy to scale up. The porous TiO_2 hollow aggregates exhibit higher photocatalytic activity than that of commercially available photocatalyst P25. The high photocatalytic activity of these TiO_2 aggregates is related to the larger surface area, smaller crystal size, and highly porous structure.

Experimental Section

Synthesis: A one-step hydrothermal preparation of the porous TiO_2 hollow aggregates was performed as follows. Typically, $Ti(SO_4)_2$ (0.346 g,

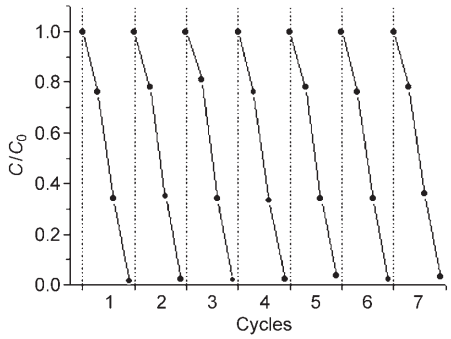

Figure 9. Cycles of the photocatalytic degradation of RhB in the presence of the porous TiO_2 hollow aggregates that have been irradiated with UV light for 50 min (TiO_2 loading = 0.3 g L^{-1}; initial concentration (C_0) of RhB = 1×10^{-5} M).

Beijing Chemical Co.) and NH_4F (0.051 g, Aldrich) were dissolved in distilled water (80 mL). After the mixture had been stirred for 30 min, the resulting solution was added to a 100 mL Teflon-lined autoclave, and the hydrothermal synthesis was conducted at 160 °C for 6 h in an electric oven. The products were collected by means of centrifugation, washed with deionized water, and dried in an oven at 100 °C.

Characterization: The morphologies were observed by using a JEOL JSM-6700F field emission scanning electron microscope and also by using a Hitachi H-800 transmission electron microscope. The composition of the products was characterized by means of powder X-ray diffraction by using a Shimadzu XRD-6000 diffractometer with $Cu_{K\alpha}$ radiation. The nitrogen adsorption-desorption isotherms were measured by using a Micromeritics ASAP2010 system. Infrared spectra were measured by using a Nicolet Magna-IR750 FTIR spectrometer. Absorption spectra were measured by using a Shimadzu UV-240 UV/Vis spectrophotometer equipped with a labsphere diffuse reflectance accessory.

Measurement of photocatalytic activity: A cylindrical Pyrex flask was used as the photoreactor vessel. The aqueous system containing RhB (1.0×10^{-5} M, 100 mL, Aldrich) and the porous TiO_2 hollow aggregates (30 mg) was magnetically stirred in the dark for 30 min to reach the adsorption equilibrium of RhB with the catalyst, and then exposed to UV light from an Upland Mineralight lamp (254 nm, 40 μW cm^{-2}). Commercially available TiO_2 (Degussa P25) was adopted as the reference with which to compare the photocatalytic activity under the same experimental conditions. UV/Vis absorption spectra were recorded at different time intervals to monitor the reaction. TOC was measured by means of a Tekmar Dohrmann Apollo 9000 TOC analyzer.

[1] A. L. Linsebigler, G. Lu, J. T. Yates, Jr., *Chem. Rev.* **1995**, *95*, 735.
[2] A. Rachel, M. Subrahmanyam, P. Boule, *Appl. Catal., B Environ.* **2002**, *37*, 301.
[3] G. S. Shephard, S. Stochenstrom, D. de Villiers, W. J. Engelbrech, G. F. S. Wessels, *Water Res.* **2002**, *36*, 140.
[4] M. Sixto, B. Julian, V. Alfonso, R. Christoph, *Appl. Catal., B* **2002**, *37*, 1.
[5] A. Fujishima, T. N. Rao, D. A. Tryk, *J. Photochem. Photobiol. C* **2000**, *1*, 1.
[6] X. D. Wang, C. J. Summers, Z. L. Wang, *Adv. Mater.* **2004**, *16*, 1215.
[7] C. X. Ji, P. C. Searson, *J. Phys. Chem. B* **2003**, *107*, 4494.
[8] F. Li, J. He, W. L. Zhou, J. B. Wiley, *J. Am. Chem. Soc.* **2003**, *125*, 16166.
[9] D. G. Shchukin, R. A. Caruso, *Chem. Mater.* **2004**, *16*, 2287.
[10] J. Jiang, A. Kucernak, *Chem. Mater.* **2004**, *16*, 1362.
[11] K. Suzuki, K. Ikari, H. Imai, *J. Am. Chem. Soc.* **2004**, *126*, 462.
[12] X. Z. Li, H. Liu, L. F. Cheng, H. J. Tong, *Environ. Sci. Technol.* **2003**, *37*, 3989.
[13] X. X. Li, Y. J. Xiong, Z. Q. Li, Y. Xie, *Inorg. Chem.* **2006**, *45*, 3493.
[14] S. H. Zhan, D. R. Chen, X. L. Jiao, C. H. Tao, *J. Phys. Chem. B* **2006**, *110*, 11199.
[15] H. G. Yu, J. G. Yu, B. Cheng, M. H. Zhou, *J. Solid State Chem.* **2006**, *179*, 349.
[16] S. J. Gregg, K. S. W. Sing, *Adsorption, Surface Area Porosity*, Academic Press, London, **1997**, pp. 111–194.
[17] Z. G. Ding, Q. Lu, P. F. Greenfield, *J. Phys. Chem. B* **2000**, *104*, 4815.
[18] J. C. Yu, L. Z. Zhang, J. G. Yu, *Chem. Mater.* **2002**, *14*, 4647.
[19] Z. Y. Liu, X. Quan, H. B. Fu, X. Y. Li, K. Yang, *Appl. Catal., B* **2004**, *52*, 33.

Received: July 27, 2006
Published online: November 29, 2006

